# Determination of Perpendicular Magnetic Anisotropy in Fe/MgO/Fe Magnetic Tunnel Junction: A DFT-Based Spin-Orbit Torque Approach

Bao-Huei Huang,<sup>1,\*</sup> Yu-Hsiang Fu,<sup>2</sup> Chao-Cheng Kaun,<sup>2</sup> and Yu-Hui Tang<sup>1,†</sup>

<sup>1</sup>Department of Physics, National Central University, Jung-Li 32001, Taiwan

<sup>2</sup>Research Center for Applied Sciences, Academia Sinica, Taipei 11529, Taiwan

(Dated: November 8, 2022)

In our JunPy package, we have successfully combined the self-consistent Hamiltonian from first-principles calculations with the nonequilibrium Green's function method to calculate the noncollinear spin torque in the nm-scale magnetic heterojunctions. The spin-orbit coupling within the first-principles calculations is included to determine the magnetic anisotropy (MA) of an Fe/MgO/Fe magnetic tunnel junction (MTJ) with a spin-orbit torque (SOT) method. The angular dependence of accumulative SOT indicates the biaxial and uniaxial MA corresponding to the in-plane and out-of-plane rotations of the free magnetization, respectively. Our results agree with the conventional MA energy calculation for a whole MTJ and provide insights into micro-spin dynamics of local magnetic moments.

#### I. INTRODUCTION

In the study of spintronics, a perpendicular magnetic anisotropy (PMA) based magnetic tunnel junctions (MTJs) is proposed as a next-generation memory device because of its high speed in writing and reading processes and low energy consumption [1]. From the theoretical point of view, the spin-spin coupling (SSC) and spin-orbit coupling (SOC) dominate the fundamental mechanism of MTJ. The exchange interaction due to SSC between two spins keeps the spins parallel or anti-parallel and results to the magnetism of materials. For electrons in solids, the electron orbitals couple to the lattice and produce bonding among them. The SOC couples the spin direction to a specified axis along with the bonding and results to magnetic anisotropy (MA). The corresponding magnetic anisotropy energy (MAE) describes the strength to rotate the spin direction away from the easy axis due to SOC.

For the MAE calculation, the energy method is usually the way to estimate the value by computing the total energy in different magnetization angles, and the energy difference between the maximum and minimum could the MAE by force theorem. Several first-principles calculations have been performed to study the interfacial PMA effect based on the energy method [2, 3]. On the other hand, the torque method is also proposed to estimate the MAE because the total energy calculation would be difficult due to the numerical stability and high precision requirement during the self-consistent process [4]. The difficulty of the torque method would be on the calculation of magnetic noncollinear system, for which the self-consistent process is usually time-consuming than collinear system due to additional degree of freedom on other spin directions. Thanks to the development of high performance computing, the noncollinear calculations are

achievable.

In addition, the combination of SSC/SOC and nonequilibrium transport by electrical voltage or current generates the spin accumulation and control the magnetization switching. For example, the current-induced spin-transfer torque (STT) is based on the spin-transfer between the spin-polarized current and the magnetization via SSC. For the current-induced spin-orbit torque (SOT), an in-plane spin-polarized current flowing through a heavy metal suffers from an effective magnetic field produced by SOC and exchanges the spin and orbital angular momentum with the free layer magnetization at the interface [5].

In this study, we develop a spin torque method to involve the calculations of current-induced STT and interfacial SOT. Our developed package JunPy [6–8] combined first-principles calculations with nonequilibrium Green's function (NEGF) formalism achieves a general and universal spin torque calculation including STT and SOT. The electronic structure is self-consistently obtained by the NEGF-DFT calculation, and the magnetotransport properties are computed by JunPy package. We employ an Fe/MgO/Fe MTJ to carry out the spin torque calculations including the current-induced STT by applying electrical bias across the junction and interfacial SOT by considering SOC in the first-principles calculation.

# II. THEORETICAL FORMALISM

#### A. System Hamiltonian

For a spin-polarized many-body system in a framework of first-principles calculations, the spin moment operator of the system is expressed as  $\hat{\vec{\mu}} = -\gamma \hat{\vec{S}}$  with  $\gamma$  being the gyromagnetic ratio and  $\hat{\vec{S}} = (\hbar/2)\hat{\vec{\sigma}}$  the spin density operator represented by the vector of Pauli matrices. In the description of non-interacting electrons, we first have

<sup>\*</sup> lise811020@gmail.com

<sup>†</sup> yhtang@cc.ncu.edu.tw

the spin-independent Hamiltonian of a  $\lambda$  orbital as

$$\hat{\mathcal{H}}^0 = \frac{\hat{\vec{p}}_{\lambda}^2}{2m} + \hat{U}_{\lambda}^{\text{eff}},\tag{1}$$

where  $\hat{\vec{p}}_{\lambda}$  is the electron momentum, m the electron mass, and  $\hat{U}_{\lambda}^{\text{eff}}$  the spin-independent effective potential. For a magnetic material, the unbalanced spin-up and -down energy states under the Fermi level cause a local magnetization  $\vec{M}_{\lambda}$ , which induces an internal exchange field  $\vec{B}_{\lambda}^{\text{XC}} = \mu_0 \vec{M}_{\lambda}$ , and the exchange coupling with the system spin is expressed as

$$\hat{\mathcal{H}}^{\text{XC}} = -\hat{\vec{\mu}} \cdot \vec{B}_{\lambda}^{\text{XC}} = J_{\lambda}^{\text{XC}} \hat{\vec{S}} \cdot \vec{M}_{\lambda}, \tag{2}$$

where the effective value  $J_{\lambda}^{\text{XC}}$  represents the coupling strength. On the other hand, the orbital angular momentum  $\hat{\vec{L}}_{\lambda}$  induces an effective field  $\hat{B}_{\lambda}^{\text{SO}}$ , and results to the spin-orbit coupling as

$$\hat{\mathcal{H}}^{SO} = -\hat{\vec{\mu}} \cdot \hat{\vec{B}}_{\lambda}^{SO} = \xi_{\lambda}^{SO} \hat{\vec{S}} \cdot \hat{\vec{L}}_{\lambda}, \tag{3}$$

where  $\xi_{\lambda}^{\rm SO}$  is an effective strength value. Finally,

$$\hat{\mathcal{H}} = \hat{\mathcal{H}}^0 + \hat{\mathcal{H}}^{XC} + \hat{\mathcal{H}}^{SO} \tag{4}$$

is a general description of the system Hamiltonian.

# B. Dynamics of local magnetization

The dynamics of the local magnetization  $M_{\lambda}$  can be classically described by the Landau-Lifshitz-Gilbert (LLG) equation [9, 10]:

$$\left. \frac{d\vec{M}_{\lambda}}{dt} \right|_{\rm LLG} = -\gamma \vec{M}_{\lambda} \times \vec{H}_{\lambda}^{\rm eff} + \frac{\alpha}{M_s} \left( \vec{M}_{\lambda} \times \frac{d\vec{M}_{\lambda}}{dt} \right). \quad (5)$$

The first term of RHS describes the precession motion due to an effective magnetic field  $\vec{H}_{\lambda}^{\text{eff}}$ . The second term with the phenomenological Gilbert damping constant  $\alpha$  describes the energy loss during precession motion. We refer these two terms as the classical LLG torques since the time derivative of an angular momentum is defined as torque. In addition to the classical terms, we also require to consider the quantum-mechanical (QM) torques exerting to the magnetization, which is described by the Heisenberg equation of motion [11]:

$$\frac{d\vec{M}_{\lambda}}{dt} \bigg|_{QM} = \frac{1}{i\hbar} \left\langle \left[ \vec{M}_{\lambda}, \hat{\mathcal{H}} \right] \right\rangle_{\lambda}$$

$$= -\gamma J_{\lambda}^{XC} \langle \hat{\vec{S}}_{\lambda} \rangle \times \vec{M}_{\lambda},$$
(6)

where  $\langle \hat{\vec{S}}_{\lambda} \rangle$  is the expectation value of the spin density operator at the  $\lambda$  orbital. The QM torques may include

the current-induced spin-transfer torque, interlayer exchange coupling, and magnetic anisotropy (due to spin-orbit torque). As a result,

$$\frac{d\vec{M}_{\lambda}}{dt} = \left. \frac{d\vec{M}_{\lambda}}{dt} \right|_{\text{LLG}} + \left. \frac{d\vec{M}_{\lambda}}{dt} \right|_{\text{QM}} \tag{7}$$

represents the dynamics of the local magnetization in the effects of classical and QM torques.

#### C. Spin continuity equation

In order to calculate the QM torques, we start from the spin continuity equation to derive the spin dynamics formulas. Introducing  $\hat{P}_{\lambda}$  and  $\hat{P}_{\lambda}^{\dagger}$  as projection operators to the  $\lambda$  orbital, the spin density operator of the  $\lambda$  orbital is obtained as

$$\hat{\vec{S}}_{\lambda} = \frac{1}{2} \left( \hat{P}_{\lambda}^{\dagger} \hat{\vec{S}} + \hat{\vec{S}} \hat{P}_{\lambda} \right), \tag{8}$$

where  $\sum_{\lambda} \hat{P}_{\lambda} = \sum_{\lambda} \hat{P}_{\lambda}^{\dagger} = \hat{I}$  satisfies the completeness relation with  $\hat{I}$  being the identity operator. Note that we first keep the difference between  $\hat{P}_{\lambda}$  and  $\hat{P}_{\lambda}^{\dagger}$  because they are not identical in the consideration of nonorthogonal basis that will be discussed later.

Using the system Hamiltonian, we have a continuity equation of the total spin density projected to a specified orbital  $\lambda$  by Heisenberg equation of motion:

$$\frac{d\vec{S}_{\lambda}}{dt} = \frac{1}{i\hbar} \left[ \hat{\vec{S}}_{\lambda}, \hat{\mathcal{H}} \right] 
= \hat{\vec{\Phi}}_{\lambda}^{S} + \hat{\vec{T}}_{\lambda}^{S},$$
(9)

where

$$\hat{\vec{\Phi}}_{\lambda}^{S} = \frac{1}{2} \left( \hat{\vec{S}} \hat{\Phi}_{\lambda} + \hat{\Phi}_{\lambda}^{\dagger} \hat{\vec{S}} \right) \tag{10}$$

$$\hat{\vec{T}}_{\lambda}^{\mathrm{S}} = \frac{1}{2} \left( \hat{P}_{\lambda}^{\dagger} \hat{\vec{T}}^{\mathrm{S}} + \hat{\vec{T}}^{\mathrm{S}} \hat{P}_{\lambda} \right) \tag{11}$$

are the operators of spin current accumulation and spin torque of the  $\lambda$  orbital, respectively. Here

$$\hat{\Phi}_{\lambda} = \frac{1}{i\hbar} \left[ \hat{P}_{\lambda}, \hat{\mathcal{H}} \right] \tag{12}$$

$$\hat{\Phi}_{\lambda}^{\dagger} = \frac{1}{i\hbar} \left[ \hat{P}_{\lambda}^{\dagger}, \hat{\mathcal{H}} \right] \tag{13}$$

are the operators of (spin-independent) current accumulation of the  $\lambda$  orbital [12], and

$$\hat{\vec{T}}^{S} = \frac{1}{i\hbar} \left[ \hat{\vec{S}}, \hat{\mathcal{H}} \right] \tag{14}$$

are introduced as an operator of total spin torque of the system [13, 14].

For the current accumulation operators  $\hat{\Phi}_{\lambda}$  and  $\hat{\Phi}_{\lambda}^{\dagger}$ , they can be also expressed by the interorbital current

(or called bonding current). Introducing the interorbital current operators between the  $\lambda'$  and  $\lambda$  orbitals as [12]

$$\hat{J}_{\lambda\lambda'} \equiv \frac{1}{i\hbar} \left( \hat{P}_{\lambda'} \hat{\mathcal{H}} \hat{P}_{\lambda} - \hat{P}_{\lambda} \hat{\mathcal{H}} \hat{P}_{\lambda'} \right) \tag{15}$$

$$\hat{J}^{\dagger}_{\lambda\lambda'} \equiv \frac{1}{i\hbar} \left( \hat{P}^{\dagger}_{\lambda'} \hat{\mathcal{H}} \hat{P}^{\dagger}_{\lambda} - \hat{P}^{\dagger}_{\lambda} \hat{\mathcal{H}} \hat{P}^{\dagger}_{\lambda'} \right), \tag{16}$$

we have

$$\hat{\Phi}_{\lambda} = \frac{1}{i\hbar} \left[ \hat{P}_{\lambda}, \hat{\mathcal{H}} \right] 
= \frac{1}{i\hbar} \left( \hat{P}_{\lambda} \hat{\mathcal{H}} \hat{I} - \hat{I} \hat{\mathcal{H}} \hat{P}_{\lambda} \right) 
= \sum_{\lambda'} \frac{1}{i\hbar} \left( \hat{P}_{\lambda} \hat{\mathcal{H}} \hat{P}_{\lambda'} - \hat{P}_{\lambda'} \hat{\mathcal{H}} \hat{P}_{\lambda} \right) 
= \sum_{\lambda' \neq \lambda} \frac{1}{i\hbar} \left( \hat{P}_{\lambda} \hat{\mathcal{H}} \hat{P}_{\lambda'} - \hat{P}_{\lambda'} \hat{\mathcal{H}} \hat{P}_{\lambda} \right) 
= -\sum_{\lambda' \neq \lambda} \hat{J}_{\lambda \lambda'},$$
(17)

where the completeness relation of projection operator is used. The same procedure is done for  $\hat{\Phi}^{\dagger}_{\lambda}$  by replacing  $\hat{P}_{\lambda}$  with  $\hat{P}^{\dagger}_{\lambda}$ . It can be identified that the current accumulation is the net flux of the interorbital current into the  $\lambda$  orbital. By defining the spin current operator between  $\lambda'$  and  $\lambda$  orbitals as

$$\hat{\vec{J}}_{\lambda\lambda'}^{S} \equiv \frac{1}{2} \left( \hat{\vec{S}} \hat{J}_{\lambda\lambda'} + \hat{J}_{\lambda\lambda'}^{\dagger} \hat{\vec{S}} \right), \tag{18}$$

the spin current accumulation [Eq. (10)] can be represented as

$$\hat{\bar{\Phi}}_{\lambda}^{S} = -\sum_{\lambda' \neq \lambda} \hat{J}_{\lambda\lambda'}^{S}, \qquad (19)$$

which corresponds to the spin version of Eq. (17).

By using the interorbital current representation, the spin continuity equation [Eq. (9)] can be expressed as

$$\frac{d\vec{S}_{\lambda}}{dt} = -\sum_{\lambda' \neq \lambda} \hat{\vec{J}}_{\lambda\lambda'}^{S} + \hat{\vec{T}}_{\lambda}^{S} . \qquad (20)$$

Here we have presented the spin current accumulation (or the net flux of spin current) in the discrete summation form. For continuous integral form, we have  $\hat{\bar{\Phi}}_{\lambda}^{\mathrm{S}} = -\oint_{A} \hat{\mathcal{J}}^{\mathrm{S}} \cdot d\vec{A}, \text{ which accounts the net flux on a close surface } A. \text{ Here } \hat{\mathcal{J}}^{\mathrm{S}} \text{ denotes the spin current tensor in both of the spin and real space. By employing the divergence theorem, the accumulation in a volume } V \text{ can also be written as } \hat{\bar{\Phi}}_{\lambda}^{\mathrm{S}} = -\int_{V} (\nabla \cdot \hat{\mathcal{J}}^{\mathrm{S}}) dV, \text{ in which the divergence form } -\nabla \cdot \hat{\mathcal{J}}^{\mathrm{S}} \text{ is more generally used to represent the continuity equation } [11, 15–17].}$ 

In the presence of SOC, we seek the corresponding contribution on the spin current accumulation and the spin

torque. By means of the individual components of the Hamiltonian,  $\hat{\Phi}_{\lambda}^{S}$  and  $\hat{T}_{\lambda}^{S}$  are respectively rewritten as

$$\hat{\bar{\Phi}}_{\lambda}^{S,X} = -\sum_{\lambda' \neq \lambda} \hat{\bar{J}}_{\lambda\lambda'}^{S,X} 
= -\sum_{\lambda' \neq \lambda} \frac{1}{2} \left( \hat{\bar{S}} \hat{J}_{\lambda\lambda'}^{X} + \hat{J}_{\lambda\lambda'}^{X\dagger} \hat{\bar{S}} \right)$$
(21)

$$\hat{J}_{\lambda\lambda'}^{X} = \frac{1}{i\hbar} \left( \hat{P}_{\lambda'} \hat{\mathcal{H}}^{X} \hat{P}_{\lambda} - \hat{P}_{\lambda} \hat{\mathcal{H}}^{X} \hat{P}_{\lambda'} \right) \tag{22}$$

$$\hat{J}_{\lambda\lambda'}^{X\dagger} = \frac{1}{i\hbar} \left( \hat{P}_{\lambda'}^{\dagger} \hat{\mathcal{H}}^{X} \hat{P}_{\lambda}^{\dagger} - \hat{P}_{\lambda}^{\dagger} \hat{\mathcal{H}}^{X} \hat{P}_{\lambda'}^{\dagger} \right) \tag{23}$$

and

$$\hat{\vec{T}}_{\lambda}^{\mathrm{S},X} = \frac{1}{2} \left( \hat{P}_{\lambda}^{\dagger} \hat{\vec{T}}^{X} + \hat{\vec{T}}^{\mathrm{S},X} \hat{P}_{\lambda} \right) \tag{24}$$

$$\hat{\vec{T}}^{S,X} = \frac{1}{i\hbar} \left[ \hat{\vec{S}}, \hat{\mathcal{H}}^X \right] \tag{25}$$

with X being the symbol of KE, XC or SO. We introduce  $\hat{\Phi}_{\lambda}^{S,KE}$  as the kinetic contribution of the spin current accumulation since it involves the spin-independent Hamiltonian  $\hat{\mathcal{H}}^0$ . On the other hand, the SOC-induced spin current accumulation  $\hat{\Phi}_{\lambda}^{S,SO}$  results from the SOC part of the Hamiltonian  $\hat{\mathcal{H}}^{SO}$  [18]. The exchange contribution  $\hat{\Phi}_{\lambda}^{S,XC}$  is zero since  $\hat{\mathcal{H}}^{XC}$  is assumed not to involve with the electron momentum. The kinetic spin torque  $\hat{T}^{S,KE}$  is also zero since  $\hat{\mathcal{H}}^0$  is spin-independent. Moreover,  $\hat{T}_{\lambda}^{S,XC}$  and  $\hat{T}_{\lambda}^{S,SO}$  are introduced as the exchange spin torque and spin-orbit torque, respectively [19]. Finally, the spin continuity equation [Eq. (9)] can be decomposed as

$$\frac{d\hat{\vec{S}}_{\lambda}}{dt} = \hat{\vec{\Phi}}_{\lambda}^{S,KE} + \hat{\vec{\Phi}}_{\lambda}^{S,SO} + \hat{\vec{T}}_{\lambda}^{S,XC} + \hat{\vec{T}}_{\lambda}^{S,SO}.$$
 (26)

For the exchange spin torque of the  $\lambda$  orbital  $\hat{T}_{\lambda}^{S,XC}$ , we can expand the commutator and express it by cross product [13]:

$$\hat{\vec{T}}_{\lambda}^{S,XC} = \frac{1}{2} \left( \hat{P}_{\lambda}^{\dagger} \hat{\vec{T}}^{S,XC} + \hat{\vec{T}}^{S,XC} \hat{P}_{\lambda} \right) 
= \frac{1}{2} \frac{1}{i\hbar} \left( \hat{P}_{\lambda}^{\dagger} \left[ \hat{\vec{S}}, \hat{\mathcal{H}}^{XC} \right] + \left[ \hat{\vec{S}}, \hat{\mathcal{H}}^{XC} \right] \hat{P}_{\lambda} \right) 
= -J_{\lambda}^{XC} \frac{1}{2} \left( \hat{P}_{\lambda}^{\dagger} \hat{\vec{S}} \times \vec{M}_{\lambda} + \hat{\vec{S}} \times \vec{M}_{\lambda} \hat{P}_{\lambda} \right) 
= -J_{\lambda}^{XC} \frac{1}{2} \left( \hat{P}_{\lambda}^{\dagger} \hat{\vec{S}} + \hat{\vec{S}} \hat{P}_{\lambda} \right) \times \vec{M}_{\lambda} 
= -J_{\lambda}^{XC} \hat{\vec{S}}_{\lambda} \times \vec{M}_{\lambda},$$
(27)

and we have the expectation value as

$$\langle \hat{\vec{T}}_{\lambda}^{\mathrm{S,XC}} \rangle = -J_{\lambda}^{\mathrm{XC}} \langle \hat{\vec{S}}_{\lambda} \rangle \times \vec{M}_{\lambda}.$$
 (28)

Comparing with Eq. (6), we can find that the QM torques is simply the exchange spin torque as

$$\frac{d\vec{M}_{\lambda}}{dt}\bigg|_{\text{OM}} = \gamma \langle \hat{\vec{T}}_{\lambda}^{\text{S,XC}} \rangle, \tag{29}$$

which has been proposed in Ref. [11, 15]. As a result, the dynamics of the local magnetization can also be computed via the exchange spin torque.

# D. Role of SOC

To account the role of SOC in the dynamics of magnetization, we assume the system is in the condition of steady state  $d_t \hat{\vec{S}}_{\lambda}(t) = 0$ . From Eq. (26) and (29), we have the magnetization dynamics represented as

$$\frac{d\vec{M}_{\lambda}}{dt} \bigg|_{QM} = \gamma \langle \hat{\vec{T}}_{\lambda}^{S,XC} \rangle 
= \gamma \left( -\langle \hat{\vec{\Phi}}_{\lambda}^{S,KE} \rangle - \langle \hat{\vec{\Phi}}_{\lambda}^{S,SO} \rangle - \langle \hat{\vec{T}}_{\lambda}^{S,SO} \rangle \right).$$
(30)

It is clear that the kinetic spin current accumulation  $\hat{\Phi}_{\lambda}^{\mathrm{S,KE}}$  flowing from other orbitals will suffer an additional SOT and an SOC-induced spin current accumulation. For the concept of SOC, it is often stated that an electron moving inside a potential V with momentum  $\hat{p}_{\lambda}$  will experience a force due to a magnetic field, which is represented as  $\hat{B}_{\lambda}^{\mathrm{SO}} \propto \nabla V \times \hat{p}_{\lambda}$  [11, 20]. Such additional force can be considered as SOT. We can also say that the spin is not conserved between  $\hat{T}_{\lambda}^{\mathrm{S,XC}}$  and  $\hat{\Phi}_{\lambda}^{\mathrm{S,KE}}$  due to the presence of SOC [5, 18]. Therefore, to account the QM toques in the magnetization dynamics, we can compute either  $\hat{T}_{\lambda}^{\mathrm{S,XC}}$  directly or  $\hat{\Phi}_{\lambda}^{\mathrm{S,KE}}$ ,  $\hat{\Phi}_{\lambda}^{\mathrm{S,SO}}$  and  $\hat{T}_{\lambda}^{\mathrm{S,SO}}$  to see the individual contribution.

In the absence of SOC, the exchange spin torque can be directly obtained from the kinetic spin current accumulation, i.e.,  $\hat{T}_{\lambda}^{\mathrm{S,XC}} = -\hat{\Phi}_{\lambda}^{\mathrm{S,KE}}.$  Such condition is employed to compute the spin torque from the spin current accumulation if the SOC effect in the system is neglectable. Note that what we say the spin current accumulation includes not only from the nonequilibrium conducting electrons but also from the equilibrium ones due to the spatial variation of spin such as a non-uniformly magnetized heterojunction. The equilibrium contribution may refer as the equilibrium field-like spin torque  $T_{\perp}^{(0)}$ , and the nonequilibrium contributes to both of the damp-like spin torque (or simply the spin-transfer torque)  $T_{\parallel}^{(V)}$  and the nonequilibrium field-like spin torque  $T_{\perp}^{(V)}$  [21–23].

#### III. FIRST-PRINCIPLES IMPLEMENTATION

#### A. Localized orbital representations

We next construct the matrix representations of the spin dynamics formulas by linear combination of atomic orbitals (LCAO) approach. The expectation value of the spin current accumulation and spin torque will be derived. Note that, in this study, an element of a matrix **O** 

is defined as  $\mathbf{O}_{mn} \equiv (\mathbf{O})_{mn}$ , and a one of the operated matrix is  $\mathbf{O}_{mn}^X \equiv (\mathbf{O}^X)_{mn}$  with  $X = \{-1, \dagger, T\}$  being the inverse, Hermitian, or transpose operation. For a spin-polarized system, a matrix element  $\mathbf{O}_{\mu\nu}$  with the orbital indices  $\mu$  and  $\nu$  is a  $2 \times 2$  submatrix in spin space. The system is expanded by a finite set of nonorthogonal atomic orbitals  $\{|\mu\rangle\}$  with the overlapping matrix element as  $\mathbf{\Omega}_{\mu\nu} = \langle \mu|\nu\rangle$  and the Hamiltonian matrix element as  $\mathbf{H}_{\mu\nu} = \langle \mu|\hat{\mathcal{H}}|\nu\rangle$ . The individual contributions  $\mathbf{H}_{\mu\nu}^0$ ,  $\mathbf{H}_{\mu\nu}^{\mathrm{XC}}$  and  $\mathbf{H}_{\mu\nu}^{\mathrm{SO}}$  are obtained as described in Appendix A. Using the overlapping matrix elements, the identity operator can be expanded as

$$\hat{I} = \sum_{\mu\nu} |\mu\rangle \mathbf{\Omega}_{\mu\nu}^{-1} \langle \nu|. \tag{31}$$

Due to the nonorthogonal property, the projection operators to the  $\lambda$  orbital have two types of form [24]:

$$\hat{P}_{\lambda} = \sum_{\nu} |\lambda\rangle \mathbf{\Omega}_{\lambda\nu}^{-1} \langle \nu| \tag{32}$$

$$\hat{P}_{\lambda}^{\dagger} = \sum_{\nu} |\nu\rangle \Omega_{\nu\lambda}^{-1} \langle \lambda|. \tag{33}$$

These operators in terms of matrix representation will be used to rewrite the spin dynamics formulas.

We also need a density matrix to compute the expectation values. The eigenvalue method is first presented here and the Green's function approach will be discussed in the next section. Using the basis set, the eigenket and eigenbra of a state n are respectively expanded as

$$|\psi_n\rangle = \sum_{\nu} |\nu\rangle \mathbf{C}_{\nu n} \tag{34}$$

$$\langle \psi_n | = \sum_{\mu} \mathbf{C}_{n\mu}^{\dagger} \langle \mu |,$$
 (35)

where  $\mathbf{C}_{\nu n}$  and  $\mathbf{C}_{n\mu}^{\dagger}$  are the expansion coefficients. In steady state, the coefficients can be solved by the eigenvalue equations:

$$\mathbf{HC} = \mathbf{\Omega} \mathbf{C} \mathbf{\Lambda}$$

$$\mathbf{C}^{\dagger} \mathbf{H} = \mathbf{\Lambda} \mathbf{C}^{\dagger} \mathbf{\Omega}$$

$$\mathbf{\Lambda} = \operatorname{diag} (\varepsilon_{1}, \varepsilon_{2}, \cdots, \varepsilon_{n}),$$
(36)

where  $\Lambda$  is a diagonal matrix filled with the eigenenergy  $\varepsilon_n$ . The elements of the density matrix  $\mathbf{D}_{\mu\nu}$  and the energy density matrix  $\mathbf{D}_{\mu\nu}^{\mathrm{E}}$  are computed by

$$\mathbf{D}_{\mu\nu} = \sum_{n} f_n \mathbf{C}_{\mu n} \mathbf{C}_{n\nu}^{\dagger} \tag{37}$$

$$\mathbf{D}_{\mu\nu}^{\mathrm{E}} = \sum_{n} f_{n} \varepsilon_{n} \mathbf{C}_{\mu n} \mathbf{C}_{n\nu}^{\dagger}, \tag{38}$$

where  $f_n$  is an occupation factor. The matrices  $\mathbf{H}$ ,  $\mathbf{\Omega}$  and  $\mathbf{D}$  required to compute the spin dynamics formulas can be constructed, for example, by first-principles calculations [13, 25] or by tight-binding models [21, 23].

Next, we show the expectation values of the spin dynamics formulas by using the LCAO represented operators above. We first have the matrix representation of the spin angular momentum operator as

$$\vec{\mathbf{S}}_{\mu\nu} = \langle \mu | \hat{\vec{S}} | \nu \rangle = \frac{\hbar}{2} \vec{\sigma} \mathbf{\Omega}_{\mu\nu}, \tag{39}$$

where  $\vec{\boldsymbol{\sigma}} = (\boldsymbol{\sigma}^x, \boldsymbol{\sigma}^y, \boldsymbol{\sigma}^z)$  is the vector of  $2 \times 2$  Pauli matrices. For the spin torque operator, the matrix elements are computed by

$$\vec{\mathbf{T}}_{\mu\nu}^{S} = \langle \mu | \hat{\vec{T}}^{S} | \nu \rangle = \frac{1}{i\hbar} \left[ \frac{\hbar}{2} \vec{\boldsymbol{\sigma}}, \mathbf{H}_{\mu\nu} \right], \tag{40}$$

and the expectation value of the  $\lambda$  orbital is derived as

$$\vec{T}_{\lambda}^{S} = \langle \hat{\vec{T}}_{\lambda}^{S} \rangle 
= \frac{1}{2} \left( \langle \hat{P}_{\lambda}^{\dagger} \hat{\vec{T}}^{S} \rangle + \langle \hat{\vec{T}}^{S} \hat{P}_{\lambda} \rangle \right) 
= \frac{1}{2} \operatorname{Tr}_{\sigma} \left( \vec{\mathbf{T}}^{S} \mathbf{D} + \mathbf{D} \vec{\mathbf{T}}^{S} \right)_{\lambda \lambda}.$$
(41)

For the spin current, we first define two quantities

$$\vec{\mathbf{F}}_{\lambda\lambda'}^{(1)} \equiv \frac{1}{i\hbar} \frac{\hbar}{2} \left[ \mathbf{D}_{\lambda\lambda'}^{(2)} \vec{\boldsymbol{\sigma}} \mathbf{H}_{\lambda'\lambda}^{(1)} + \mathbf{D}_{\lambda\lambda'}^{(1)} \mathbf{H}_{\lambda'\lambda}^{(2)} \vec{\boldsymbol{\sigma}} \right]$$
(42)

$$\vec{\mathbf{F}}_{\lambda\lambda'}^{(2)} \equiv \frac{1}{i\hbar} \frac{\hbar}{2} \left[ \vec{\boldsymbol{\sigma}} \mathbf{H}_{\lambda\lambda'}^{(1)} \mathbf{D}_{\lambda'\lambda}^{(2)} + \mathbf{H}_{\lambda\lambda'}^{(2)} \vec{\boldsymbol{\sigma}} \mathbf{D}_{\lambda'\lambda}^{(1)} \right], \tag{43}$$

where we have used the definition

$$\mathbf{H}^{(1)} \equiv \mathbf{\Omega}^{-1} \mathbf{H} \qquad \mathbf{D}^{(1)} \equiv \mathbf{\Omega} \mathbf{D} 
\mathbf{H}^{(2)} \equiv \mathbf{H} \mathbf{\Omega}^{-1} \qquad \mathbf{D}^{(2)} \equiv \mathbf{D} \mathbf{\Omega} , \tag{44}$$

and the expectation value is derived as

$$\vec{J}_{\lambda\lambda'}^{S} = \langle \hat{J}_{\lambda\lambda'}^{S} \rangle 
= \frac{1}{2} \left( \langle \hat{\vec{S}} \hat{J}_{\lambda\lambda'} \rangle + \langle \hat{J}_{\lambda\lambda'}^{\dagger} \hat{\vec{S}} \rangle \right) 
= \frac{1}{2} \text{Tr}_{\sigma} \left( \vec{\mathbf{F}}_{\lambda\lambda'}^{(1)} - \vec{\mathbf{F}}_{\lambda\lambda'}^{(2)} \right).$$
(45)

Finally, the spin current accumulation is

$$\vec{\Phi}_{\lambda}^{S} = \langle \hat{\vec{\Phi}}_{\lambda}^{S} \rangle = -\sum_{\lambda' \neq \lambda} \langle \hat{\vec{J}}_{\lambda \lambda'}^{S} \rangle. \tag{46}$$

Here the spin current equations seem not intuitive because of the existing  $\Omega$  and  $\Omega^{-1}$ . If the system is expanded by an orthogonal basis set, i.e.,  $\Omega = \Omega^{-1} = I$ , then Eq. (45) is simplified as

$$\vec{J}_{\lambda\lambda'}^{\text{S,orth}} = \frac{1}{2} \text{Tr}_{\sigma} \left( \mathbf{D}_{\lambda\lambda'} \vec{\mathbf{J}}_{\lambda'\lambda}^{\text{orth}} - \vec{\mathbf{J}}_{\lambda\lambda'}^{\text{orth}} \mathbf{D}_{\lambda'\lambda} \right), \tag{47}$$

where

$$\vec{\mathbf{J}}_{\lambda'\lambda}^{\text{orth}} = \frac{1}{i\hbar} \left\{ \frac{\hbar}{2} \vec{\boldsymbol{\sigma}}, \mathbf{H}_{\lambda'\lambda} \right\}. \tag{48}$$

It shows that the commutator in the calculation of spin torque [Eq. (40)] is replaced by the anti-commutator in the spin current calculation [Eq. 48]. Also, the addition property of Eq. (41) becomes the subtraction in Eq. (47). Such relation can also be found in the representation of wave function formalism [19].

#### B. NEGF formalism

So far, the spin dynamics formulas have been derived in terms of the density matrix. For applications with two-probe structures, we make use of the Keldysh nonequilibrium Green's function (NEGF) formalism to compute the density matrix [25–27]. In steady state, the retarded Green's function is computed via

$$\mathbf{G}^{r}\left(E\right) = \left[E\mathbf{\Omega} - \mathbf{H} - \mathbf{\Sigma}_{\mathrm{B}}^{r}\left(E^{+}\right) - \mathbf{\Sigma}_{\mathrm{T}}^{r}\left(E^{+}\right)\right]^{-1}, \quad (49)$$

where  $E^+ = E + i\eta$  with  $\eta$  being an infinitesimal positive number. Also,  $\mathbf{G}^a = (\mathbf{G}^r)^{\dagger}$  is the advanced Green's function and  $\mathbf{\Sigma}_{\mathrm{B}(\mathrm{T})}^r$  is the self-energy matrix of the bottom (top) electrode. Given the Keldysh Green's function  $\mathbf{G}^< = \mathbf{G}^r \mathbf{\Sigma}^< \mathbf{G}^a$  and the lesser self-energy  $\mathbf{\Sigma}^< = i (f_{\mathrm{B}} \mathbf{\Gamma}_{\mathrm{B}} + f_{\mathrm{T}} \mathbf{\Gamma}_{\mathrm{T}})$  with  $\mathbf{\Gamma}_{\mathrm{B}(\mathrm{T})} = i (\mathbf{\Sigma}_{\mathrm{B}(\mathrm{T})}^r - \mathbf{\Sigma}_{\mathrm{B}(\mathrm{T})}^a)$  being the broadening function of the bottom (top) electrode, we have the density matrix and energy density matrix as

$$\mathbf{D}_{\mu\nu} = -i \int \frac{dE}{2\pi} \mathbf{G}_{\mu\nu}^{<}(E)$$
 (50)

$$\mathbf{D}_{\mu\nu}^{\mathrm{E}} = -i \int \frac{dE}{2\pi} E \mathbf{G}_{\mu\nu}^{<}(E). \tag{51}$$

If the system is in equilibrium, the Keldysh Green's function can be simply expressed as [26]

$$\mathbf{G}^{<}\left(E\right) = f\left(E\right)\left[\mathbf{G}^{a}\left(E\right) - \mathbf{G}^{r}\left(E\right)\right] \tag{52}$$

and the density matrices are thus

$$\mathbf{D}_{\mu\nu}^{\mathrm{eq}} = -i \int \frac{dE}{2\pi} f\left(E\right) \left[ \mathbf{G}_{\mu\nu}^{a}\left(E\right) - \mathbf{G}_{\mu\nu}^{r}\left(E\right) \right]$$
 (53)

$$\mathbf{D}_{\mu\nu}^{\mathrm{E,eq}} = -i \int \frac{dE}{2\pi} Ef(E) \left[ \mathbf{G}_{\mu\nu}^{a}(E) - \mathbf{G}_{\mu\nu}^{r}(E) \right]$$
 (54)

where f(E) is the Fermi-Dirac distribution function. The energy integration of the equilibrium density matrices can be performed efficiently by integrating along a complex contour [25].

# IV. CALCULATION DETAILS

A conventional magnetic tunnel junction Fe/MgO/Fe is employed to study the spin dynamics, and the structure is the same with our previous calculation [7]. We construct the system by a two-probe structure, in which the MgO insulator is sandwiched by two semi-infinite bcc-Fe electrodes as shown in Fig. 1. The composition Fe(7)/MgO(5)/Fe(6), where the numbers are the number of atomic layers, is chosen as the central scattering region. The structure of the electrodes and scattering region are optimized using the density function theory (DFT) based VASP package [28, 29] with the projector augmented wave (PAW) pseudopotential and PBE exchange correlation functional [30]. The energy cutoff for

the plane-wave-basis set is 700 eV, and the Brillouin zone sampling is  $31\times31\times1$  Monkhorst-Pack grid. The lattice constant of the transverse x-y plane is fixed with the optimized Fe bulk value, i.e., a=b=2.84 Å, and the optimized length of the longitudinal z direction is c=30.32 Å. Also, the optimized distance of the interfacial Fe and MgO atomic layers is 2.24 Å.

Given the optimized structure, we next obtain the selfconsistent electronic structure by using the DFT-NEGF based Nanodcal package [25, 31], where the double- $\zeta$ double-polarized LCAO basis set is used to construct the Hamiltonian and overlapping matrices. Meanwhile, the exchange-correlation functional is based on the local spin density approximation (LSDA), in which the direction of a local magnetization is locally related to the spin-splitting [16, 32]. The Brillouin zone sampling of the semi-infinite electrodes and the scattering region are respectively taken as  $15 \times 15 \times 100$  and  $15 \times 15 \times 1$ Monkhorst-Pack grid. To perform the study of noncollinear system, the magnetization direction of the bottom Fe electrode is fixed along the x-axis, and the top is freely rotated either in the z-x plane (out-of-plane) by an angle  $\theta$  or in the x-y plane (in-plane) by an angle  $\phi$ . For nonequilibrium system without SOC, the chemical potentials of the two electrodes are shifted as  $\mu_T - \mu_B = eV_b$  by a positive external bias  $V_b$ . For equilibrium system, the SOC based on the method of Ref. [33] is also included. Here the Hamiltonian and band energy are self-consistent up to  $10^{-6}$  eV for nonequilibrium and equilibrium SOC in-plane systems. For the equilibrium SOC out-of-plane system, the value  $10^{-4}$  eV is achieved. Note that the cri-

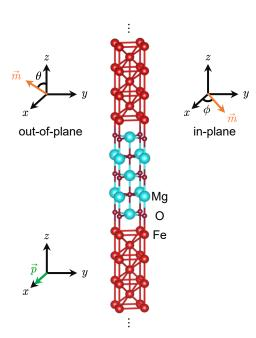


FIG. 1. The atomic structure of Fe/MgO/Fe MTJ. The magnetization of the bottom Fe electrode is fxied and the top is freely rotated either in-plane or out-of-plane.

teria depend on the difficulty of the self-consistent process. Also note that the self-consistent can't be achieved together with the SOC and external bias, and thus the case is not discussed in this study.

Finally, the physical quantities including the spin current accumulation and spin torque are calculated by our developed JunPy package using the self-consistent Hamiltonian above [34]. Also, the divide-and-conquer (DC) technique is used to study the atom-resolved quantities in the semi-infinite electrodes [7]. The complex contour energy integral method is employed for the equilibrium part of the density matrix, and the nonequilibrium part is taken over the real axis [25]. For the Brillouin zone sampling, the crystal symmetry for the system without SOC is used to reduce the sampling points while those with SOC is not reduced because the physical values in that k-space are not assumed to be symmetrized [35].

#### V. RESULTS

# A. Spin-transfer torque calculation

In the top of Fig. 2, we display the results of damplike  $(\phi)$  spin torque  $T_{\parallel}$  and spin current accumulation  $\Phi_{\parallel}$  without SOC. The results may be fixed in some conditions including the thickness  $t_m$ , bias  $V_b$  and in-plane angle  $\phi$ . In the angular [Fig. 2(a)] and bias dependency [Fig. 2(b)], we observe the kinetic spin current accumulation is the main contribution of the exchange spin torque. The spin-transfer effect has been stated that in nonzero bias the spin current flowing from the fixed layer will transfer the spin angular momentum with the free layer and result to the spin accumulation at the interface. Such spin accumulation may switch the magnetization direction of the free layer and is used to determine the currentinduced STT [16, 36, 37]. The mechanism for the sinusoidal angular and linear bias dependency can be generally discussed by the competition between the parallel and anti-parallel spin current in a tight-binding model [21]. For the layer dependency [Fig. 2(c)], both of the spin torque and spin current accumulation decay rapidly from the MgO/Fe interface indicating that most of the spin is absorbed at the interface. As a result, magnetic thin films are usually the choice to preserve the efficiency of current-induced STT [7].

In the bottom of Fig. 2, we display the results of field-like (z) spin torque  $T_{\perp}$  and spin current accumulation  $\Phi_{\perp}$  without SOC. Same with  $T_{\parallel}$ , the kinetic spin current accumulation is the main contribution of the exchange spin torque, and decays rapidly from the MgO/Fe interface. The field-like components is related to the interlayer exchange coupling (IEC) [22, 23], i.e., the exchange interaction between the two electrodes. In Fig. 2(f) the result at zero bias  $T_{\perp}^{(0)}$  demonstrates that the occupied states mainly contribute to IEC while the current-induced contribution  $T_{\perp}^{(V)}$  is weak comparing with  $T_{\parallel}$ . The exchange

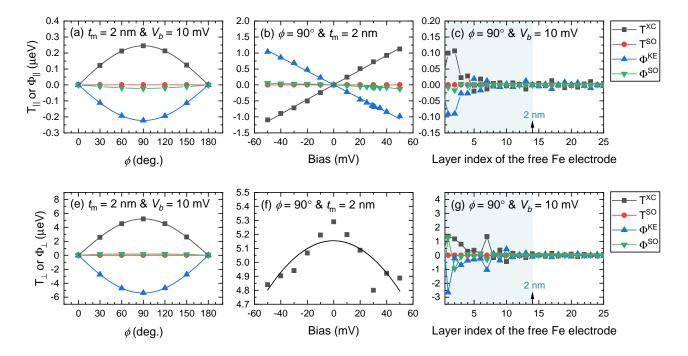


FIG. 2. The spin torque T and spin current accumulation  $\Phi$  in the damp-like (top) and field-like (bottom) direction without SOC. The angular dependency (left) with thickness  $t_m=2$  nm and bias  $V_b=10$  mV, in which the curves are fitted by sine function. The bias dependency (middle) with in-plane angle  $\phi=90^\circ$  and  $t_m=2$  nm. The curves are fitted by linear or quadratic function. The layer-resolved (right) with  $\phi=90^\circ$  and  $V_b=10$  mV.

interaction between the two electrodes means that  $T_{\perp}$  can be related to the Heisenberg-like exchange energy as [38]

$$U_{\rm IEC}(\phi) = -K_1^{\rm IEC}\cos\phi + K_2^{\rm IEC}\cos^2\phi + \cdots, \quad (55)$$

and the corresponding torque is

$$T_{\rm IEC}(\phi) \propto -\frac{\partial U_{\rm IEC}}{\partial \phi} = -K_1^{\rm IMA} \sin \phi,$$
 (56)

where  $K_1^{\rm IEC}$  is an energy constant. The high order terms may be canceled in the tunneling system, and the angular results Fig. 2(a) agree with the  $\sin \phi$  description.

# B. Spin-orbit torque calculation

Figure 3 displays the results of spin torque and spin current accumulation in the presence of SOC. The calculated angular dependence accumulated within the  $t_m=2$  nm Fe free electrode are shown in Fig. 3(c) and Fig. 3(d) for in-plane and out-of-plane rotations, respectively. It is clear that the SOC-assisted  $T^{\rm SO}$  mainly contributes to  $T^{\rm XC}$  and is in the order of meV. The nonzero value only appears in the field-like direction, i.e., z and y for in-plane and out-of-plane, respectively. Without external electric bias,  $\Phi^{\rm KE}$  and  $\Phi^{\rm SO}$  have no contribution comparing to  $T^{\rm SO}$ . Meanwhile, for the spin torque, the  $\sin 4\phi$  behavior for the in-plane case and the  $\sin 2\theta$  for the out-of-plane case are observed. For the layer dependency

shown in Fig. 3(e) and Fig. 3(f), the spin torques decay rapidly far from the MgO/Fe interface, which verifies that the broken symmetry dominates the interfacial spin-orbit torque.

In order to understand the mechanism of the angular dependent  $T^{\rm SO}$ , we tune our discussion to MA, which origins from SOC. For the in-plane case shown in Fig. 3(a), the in-plane orbital hybridization at the MgO/Fe interface implies that the cubic anisotropy of bcc-Fe bulk determines the in-plane magnetic anisotropy (IMA) energy as a biaxial form of

$$U_{\rm IMA}(\phi) = K_1^{\rm IMA} \sin^2 \phi \cos^2 \phi + \cdots, \qquad (57)$$

and the corresponding torque is

$$T_{\rm IMA}(\phi) \propto \frac{\partial U_{\rm IMA}}{\partial \phi} = \frac{1}{2} K_1^{\rm IMA} \sin 4\phi,$$
 (58)

where  $K_1^{\text{IMA}}$  is an energy constant. As for the outof-plane case in Fig. 3(b), it has been known that at the MgO/Fe interface the hybridization between Fe- $d_{z^2}$ and O- $p_z$  orbital contributes to a perpendicular magnetic anisotropy (PMA) [39, 40], which is generally described by a uniaxial magnetic anisotropy

$$U_{\text{PMA}}(\theta) = K_1^{\text{PMA}} \sin^2 \theta + \cdots, \qquad (59)$$

and the corresponding torque is

$$T_{\rm PMA}(\theta) \propto \frac{\partial U_{\rm PMA}}{\partial \theta} = K_1^{\rm PMA} \sin 2\theta.$$
 (60)

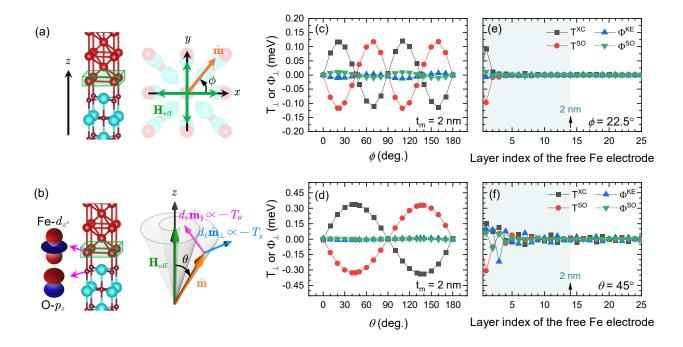


FIG. 3. (a) In-plane view and (b) out-of-plane view of the free layer magnetization in an effective magnetic field. The fields are presented by biaxial and uniaxial magnetic anisotropy, respectively. Angular dependence of spin torque and spin current accumulation in the  $t_m=2$  nm Fe electrode for (c) in-plane and (d) out-of-plane rotations. Layer-resolved spin torque and spin current accumulation at (e)  $\phi=22.5^{\circ}$  and (f)  $\theta=45^{\circ}$ . Note that the nonzero values only appears in the field-like (perpendicular,  $\perp$ ) direction in both cases.

It is clear that the  $\sin 4\phi$  and  $\sin 2\theta$  curvatures agree with our  $T^{\rm XC}$  calculation for in-plane and out-of-plane case, respectively.

# VI. DISCUSSION

In order to verify our implementation, a simple PMA system by using MgO(1)/Fe(1) bilayer shown in Fig. 4(a) is employed to compare the energy and spin torque method. Here the length of c-axis is 21.87 Å and the Fe magnetization direction is rotated by an angle  $\theta$  in the zx plane. In the Nanodcal DFT calculation, the extremely high precision using the real-space and k-space mesh cutoff to be 450 Hartree and 240 Bohr, respectively, ensure the total energy calculation precisely. We present the total energy difference defined as  $\Delta E(\theta) = E(\theta) - E(0)$  in Fig. 4(b) and the field-like (y) spin torque in Fig. 4(c). It is clear that the  $\sin^2 \theta$  [Eq. (59)] and  $\sin 2\theta$  [Eq. (60)] curvatures agree with our  $\Delta E$  and  $T^{\rm XC}$  calculation, respectively. Also, the two methods approximately exhibit the same energy value  $K_1^{\rm PMA} \sim 0.8$  meV. In the consideration of exchange-correlation energy functional, we observe a fine distinction in the total energy calculation between LDA and GGA approach while the spin torque calculation doesn't exhibit such distinction.

## VII. CONCLUSION

In this work, we have developed a spin dynamics theory to perform the calculation of spin torque and spin current accumulation in the framework of first-principles calculations including the scheme of nonequilibrium magnetotransport and spin-orbit coupling. Our implementation is applied to study the current-induced STT and the interfacial SOT in the Fe/MgO/Fe magnetic tunnel junction. The SOT calculation is employed to investigate the strength of interfacial MA energy.

# ACKNOWLEDGMENTS

This work was supported by the National Science and Technology Council, Taiwan (NSTC 108-2628-M-008-004-MY3/111-2112-M-008-025/111-2112-M-001-081/110-2923-M-001-003-MY3), the National Center for Theoretical Sciences and the National Center for Highperformance Computing for providing computational and storage resources.

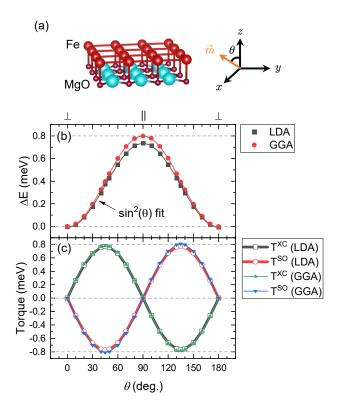


FIG. 4. (a) The atomic structure of a MgO(1)/Fe(1) bilayer, where the magnetization direction of Fe atom is rotated by an angle  $\theta$ . (b) The total energy difference defined as  $\Delta E(\theta) =$  $E(\theta) - E(0)$  for the whole system and (c) the spin torque of the Fe atom in the field-like direction.

# Appendix A: Extracting Hamiltonian components

Given a total (spin-dependent) Hamiltonian matrix from first-principles calculations

$$\mathbf{H} = \mathbf{H}^0 + \mathbf{H}^{XC} + \mathbf{H}^{SO}, \tag{A1}$$

we seek to find a simple way to separate the spinindependent, exchange and spin-orbit contributions efficiently. For simplicity, we omit the orbital index  $\mu$  and  $\nu$  in the following derivation since the same operation are applied to each  $\mathbf{H}_{\mu\nu}$ , which is a  $2\times 2$  matrix in spin space.

For the spin-independent part  $\mathbf{H}^0$ , it is approximately obtained by taking the spin-average between the spin-up and -down components [18, 41, 42]:

$$\mathbf{H}^0 \approx \frac{1}{2} \left( \mathbf{H}_{\uparrow \uparrow} + \mathbf{H}_{\downarrow \downarrow} \right) \boldsymbol{\sigma}^0,$$
 (A2)

[1] S. Ikeda, K. Miura, H. Yamamoto, K. Mizunuma, H. D. Gan, M. Endo, S. Kanai, J. Hayakawa, F. Matsukura, and H. Ohno, A perpendicular-anisotropy CoFeB-MgO magnetic tunnel junction, Nature Materials 9, 721

where  $\sigma^0$  is a 2 × 2 identity matrix. For the spindependent parts including  $\mathbf{H}^{XC}$  and  $\mathbf{H}^{SO}$ , it has been shown that [33] the spin Hamiltonian without spin-orbit contribution satisfies the Hermitian property as

$$\mathbf{H}_{\sigma\sigma'}^{\mathrm{XC}} = \left(\mathbf{H}_{\sigma'\sigma}^{\mathrm{XC}}\right)^*,\tag{A3}$$

 $\mathbf{H}^{\mathrm{XC}}_{\sigma\sigma'} = \left(\mathbf{H}^{\mathrm{XC}}_{\sigma'\sigma}\right)^*,$  and the spin-orbit contribution satisfies the Hermitian property as

$$\mathbf{H}_{\sigma\sigma'}^{SO} = -\left(\mathbf{H}_{\sigma'\sigma}^{SO}\right)^*,\tag{A4}$$

where  $\sigma$  and  $\sigma'$  denote the index of spin-up or -down. With these properties, the spin Hamiltonian can be uniquely assumed as

$$\mathbf{H}^{\mathrm{XC}} = \begin{pmatrix} a & c+id \\ c-id & b \end{pmatrix} \tag{A5}$$

$$\mathbf{H}^{SO} = \begin{pmatrix} i\alpha & \gamma + i\delta \\ -\gamma + i\delta & i\beta \end{pmatrix}, \tag{A6}$$

where the parameters  $\{a, b, c, d\}$  and  $\{\alpha, \beta, \gamma, \delta\}$  are to be determined. Given the total and spin-independent Hamiltonian, the spin-dependent part can be expressed

$$\mathbf{H}^{S} = \mathbf{H} - \mathbf{H}^{0}$$

$$= \mathbf{H}^{XC} + \mathbf{H}^{SO}$$
(A7)

$$=\begin{pmatrix} a+i\alpha & (c+\gamma)+i\left(d+\delta\right) \\ (c-\gamma)-i\left(d-\delta\right) & b+i\beta \end{pmatrix}.$$

With the expressions

$$\mathbf{H}_{\uparrow\downarrow}^{S} + \mathbf{H}_{\downarrow\uparrow}^{S} = 2c + 2i\delta$$
  
$$\mathbf{H}_{\uparrow\downarrow}^{S} - \mathbf{H}_{\downarrow\uparrow}^{S} = 2\gamma + 2id'$$
(A8)

we can find that the parameters can be determined by

$$a = \operatorname{Re} \left( \mathbf{H}_{\uparrow \uparrow}^{S} \right)$$

$$b = \operatorname{Re} \left( \mathbf{H}_{\downarrow \downarrow}^{S} \right)$$

$$c = \operatorname{Re} \left( \mathbf{H}_{\uparrow \downarrow}^{S} + \mathbf{H}_{\downarrow \uparrow}^{S} \right) / 2$$

$$d = \operatorname{Im} \left( \mathbf{H}_{\uparrow \downarrow}^{S} - \mathbf{H}_{\downarrow \uparrow}^{S} \right) / 2$$
(A9)

and

$$\alpha = \operatorname{Im} \left( \mathbf{H}_{\uparrow \uparrow}^{S} \right)$$

$$\beta = \operatorname{Im} \left( \mathbf{H}_{\downarrow \downarrow}^{S} \right)$$

$$\gamma = \operatorname{Re} \left( \mathbf{H}_{\uparrow \downarrow}^{S} - \mathbf{H}_{\downarrow \uparrow}^{S} \right) / 2$$

$$\delta = \operatorname{Im} \left( \mathbf{H}_{\uparrow \downarrow}^{S} + \mathbf{H}_{\downarrow \uparrow}^{S} \right) / 2$$
(A10)

(2010).

[2] S. Peng, M. Wang, H. Yang, L. Zeng, J. Nan, J. Zhou, Y. Zhang, A. Hallal, M. Chshiev, K. L. Wang, Q. Zhang, and W. Zhao, Origin of interfacial perpendicu-

- lar magnetic anisotropy in MgO/CoFe/metallic capping layer structures, Scientific Reports 5, 10.1038/srep18173 (2015).
- [3] S. Peng, W. Zhao, J. Qiao, L. Su, J. Zhou, H. Yang, Q. Zhang, Y. Zhang, C. Grezes, P. K. Amiri, and K. L. Wang, Giant interfacial perpendicular magnetic anisotropy in MgO/CoFe/capping layer structures, Applied Physics Letters 110, 072403 (2017).
- [4] X. Wang, R. Wu, D. sheng Wang, and A. J. Freeman, Torque method for the theoretical determination of magnetocrystalline anisotropy, Physical Review B 54, 61 (1996).
- [5] A.Manchon, J. Železný, I. Miron, T. Jungwirth, J. Sinova, A. Thiaville, K. Garello, and P. Gambardella, Current-induced spin-orbit torques in ferromagnetic and antiferromagnetic systems, Rev. Mod. Phys. 91 (2019).
- [6] The detailed information of JunPy package can be found at the website, https://labstt.phy.ncu.edu.tw/ junpy/.
- [7] B.-H. Huang, C.-C. Chao, and Y.-H. Tang, Thickness dependence of spin torque effect in fe/MgO/fe magnetic tunnel junction: Implementation of divide-and-conquer with first-principles calculation, AIP Adv. 11, 015036 (2021).
- [8] Y.-H. Tang and B.-H. Huang, Underlying mechanism for exchange bias in single-molecule magnetic junctions, Phys. Rev. Res. 3 (2021).
- [9] L. Landau and E. Lifshitz, On the theory of the dispersion of magnetic permeability in ferromagnetic bodies, in Perspectives in Theoretical Physics (Elsevier, 1992) pp. 51–65.
- [10] T. Gilbert, Classics in magnetics a phenomenological theory of damping in ferromagnetic materials, IEEE Trans. Magn. 40, 3443 (2004).
- [11] A. Manchon and S. Zhang, Theory of spin torque due to spin-orbit coupling, Phys. Rev. B 79 (2009).
- [12] T. N. Todorov, Tight-binding simulation of currentcarrying nanostructures, J. Phys.: Condens. Matter 14, 3049 (2002).
- [13] P. M. Haney, D. Waldron, R. A. Duine, A. S. Núñez, H. Guo, and A. H. MacDonald, Current-induced order parameter dynamics: Microscopic theory applied to Co/Cu/Co spin valves, Phys. Rev. B 76 (2007).
- [14] A. Kalitsov, I. Theodonis, N. Kioussis, M. Chshiev, W. H. Butler, and A. Vedyayev, Spin-polarized currentinduced torque in magnetic tunnel junctions, J. Appl. Phys. 99, 08G501 (2006).
- [15] S. Zhang and Z. Li, Roles of nonequilibrium conduction electrons on the magnetization dynamics of ferromagnets, Phys. Rev. Lett. 93 (2004).
- [16] D. Ralph and M. Stiles, Spin transfer torques, J. Magn. Magn. Mater. 320, 1190 (2008).
- [17] E. Y. Tsymbal and I. Žutić, Spintronics Handbook: Spin Transport and Magnetism, Second Edition, edited by E. Y. Tsymbal and I. Žutić (CRC Press, 2019).
- [18] A. Kalitsov, S. A. Nikolaev, J. Velev, M. Chshiev, and O. Mryasov, Intrinsic spin-orbit torque in a single-domain nanomagnet, Phys. Rev. B 96 (2017).
- [19] D. Go, F. Freimuth, J.-P. Hanke, F. Xue, O. Gomonay, K.-J. Lee, S. Blügel, P. M. Haney, H.-W. Lee, and Y. Mokrousov, Theory of current-induced angular momentum transfer dynamics in spin-orbit coupled systems, Phys. Rev. Res. 2 (2020).
- [20] Y.-H. Tang, B.-H. Huang, and M.-H. Tsai, Implementa-

- tion of the relativistic effects on spin in first-principles electronic structure and magnetic property calculations, Chin. J. Phys. **77**, 1579 (2022).
- [21] I. Theodonis, N. Kioussis, A. Kalitsov, M. Chshiev, and W. H. Butler, Anomalous bias dependence of spin torque in magnetic tunnel junctions, Phys. Rev. Lett. 97 (2006).
- [22] Y.-H. Tang, N. Kioussis, A. Kalitsov, W. H. Butler, and R. Car, Controlling the nonequilibrium interlayer exchange coupling in asymmetric magnetic tunnel junctions, Phys. Rev. Lett. 103, 057206 (2009).
- [23] Y.-H. Tang, N. Kioussis, A. Kalitsov, W. H. Butler, and R. Car, Influence of asymmetry on bias behavior of spin torque, Phys. Rev. B 81 (2010).
- [24] M. Soriano and J. J. Palacios, Theory of projections with nonorthogonal basis sets: Partitioning techniques and effective hamiltonians, Phys. Rev. B 90 (2014).
- [25] J. Taylor, H. Guo, and J. Wang, Ab initio modeling of quantum transport properties of molecular electronic devices, Phys. Rev. B 63 (2001).
- [26] S. Datta, Electronic Transport in Mesoscopic Systems, Cambridge Studies in Semiconductor Physics and Microelectronic Engineering (Cambridge University Press, 1995).
- [27] M. Brandbyge, J.-L. Mozos, P. Ordejón, J. Taylor, and K. Stokbro, Density-functional method for nonequilibrium electron transport, Phys. Rev. B 65 (2002).
- [28] G. Kresse and J. Furthmüller, Efficient iterative schemes for ab inition total-energy calculations using a plane-wave basis set, Phys. Rev. B 54, 11169 (1996).
- [29] G. Kresse and D. Joubert, From ultrasoft pseudopotentials to the projector augmented-wave method, Phys. Rev. B 59, 1758 (1999).
- [30] J. P. Perdew, K. Burke, and M. Ernzerhof, Generalized gradient approximation made simple, Phys. Rev. Lett. 77, 3865 (1996).
- [31] D. Waldron, L. Liu, and H. Guo, Ab initio simulation of magnetic tunnel junctions, Nanotechnology 18, 424026 (2007).
- [32] P. Haney, R. Duine, A. Núñez, and A. MacDonald, Current-induced torques in magnetic metals: Beyond spin-transfer, J. Magn. Magn. Mater. 320, 1300 (2008).
- [33] L. Fernández-Seivane, M. A. Oliveira, S. Sanvito, and J. Ferrer, On-site approximation for spin-orbit coupling in linear combination of atomic orbitals density functional methods, J. Phys.: Condens. Matter 18, 7999 (2006).
- [34] Y.-H. Tang and B.-H. Huang, Manipulation of giant field-like spin torque in amine-ended single-molecule magnetic junctions, J. Phys. Chem. C 122, 20500 (2018).
- [35] K.-S. Lee, D. Go, A. Manchon, P. M. Haney, M. D. Stiles, H.-W. Lee, and K.-J. Lee, Angular dependence of spinorbit spin-transfer torques, Phys. Rev. B 91 (2015).
- [36] M. D. Stiles and A. Zangwill, Anatomy of spin-transfer torque, Phys. Rev. B 66 (2002).
- [37] J. C. Slonczewski, Currents, torques, and polarization factors in magnetic tunnel junctions, Phys. Rev. B 71 (2005).
- [38] J. C. Slonczewski, Mechanism of interlayer exchange in magnetic multilayers, J. Magn. Magn. Mater. 126, 374 (1993).
- [39] H. X. Yang, M. Chshiev, B. Dieny, J. H. Lee, A. Manchon, and K. H. Shin, First-principles investigation of the very large perpendicular magnetic anisotropy at Fe/MgO and Co/MgO interfaces, Phys. Rev. B 84, 054401 (2011).

- [40] B. Dieny and M. Chshiev, Perpendicular magnetic anisotropy at transition metal/oxide interfaces and applications, Rev. Mod. Phys. 89, 025008 (2017).
- [41] T. P. Pareek and P. Bruno, Spin coherence in a two-
- dimensional electron gas with rashba spin-orbit interaction, Phys. Rev. B  ${\bf 65}$  (2002).
- [42] I. Theodonis, A. Kalitsov, and N. Kioussis, Enhancing spin-transfer torque through the proximity of quantum well states, Phys. Rev. B 76 (2007).